Intramolecular Excimer Kinetics of Fluorescent Dipyrenyl Lipids: 1. DMPC/Cholesterol Membranes

Kwan Hon Cheng,* Lucy Ruymgaart,* Lin-I Liu,* Pentti Somerharju,‡ and Istvan P. Sugar§
*Department of Physics, Texas Tech University, Lubbock, Texas 79409; ‡Department of Medical Chemistry, University of Helsinki, 00170 Helsinki, Finland; and §Departments of Biomathematical Sciences and Physiology & Biophysics, The Mount Sinai Medical Center, New York, New York 10029 USA

ABSTRACT The intramolecular dynamics of the excimer forming dipyrenyl lipids ($Dipy_nPC$) of different chain lengths (n) in ethanol and in dimyristoylphosphatidycholine (DMPC) membranes was investigated by the use of frequency-domain fluorescence intensity decay technique. Based on a 3-state model, the extent of aggregation and rotational rate of the two intralipid pyrene moieties in the dipyrenyl lipids were estimated from the frequency-domain data. In ethanol (20°C), the rotational rate for $Dipy_nPC$ increased progressively as n was varied from 4 to 12. At the gel (L_β)-to-liquid crystalline (L_α) phase transition of DMPC (~23°C), the rotational rate increased and aggregation decreased significantly for $Dipy_{10}PC$, whereas only the rotational rate was changed for $Dipy_4PC$. In the presence of 30 mol% cholesterol, significant increases in both the rotational rate and aggregation were observed for $Dipy_{10}PC$ in both L_β and L_α phases. However, for the case of $Dipy_4PC$, an increase in the rotational rate but a decrease in the aggregation were noticed only in the L_β phase, and no similar changes were detected in the L_α phase. Our results indicate differential effects of cholesterol on the conformational dynamics of acyl chains at different depths of the membranes.

INTRODUCTION

Lipophilic fluorescent probes have been used extensively to explore the conformational dynamics of membranes for several decades. Because of the sensitivity and selectivity of these probes, valuable information pertaining to the rotational and lateral diffusion mobility, as well as the orientational order, of the lipid molecules in the native and pure bilayer membranes has been accumulated. Because the fluorescence lifetimes of most commonly used lipophilic probes fall into the range of $1–100 \times 10^{-9}$ s (Lakowicz, 1983; Gratton et al., 1984), the slow dynamics (Brown et al., 1983; Bloom and Sternin, 1987; Peng et al., 1988) of the membranes, such as the collective density fluctuations of the lipids and overall rotation of the membrane vesicles, can safely be ignored (Cheng, 1989a).

Lipophilic fluorescent probes can roughly be classified into two major groups, rotational (see Cheng, 1989a–c and references therein) and lateral (see Sugar (1991) and references therein) diffusion sensitive probes. For examples, diphenylhexatriene (DPH) and its analogs belong to the first group, whereas pyrene and its analogs belong to the second group. Several previous studies (Knao et al., 1981; Chong and Thompson, 1985; Hresko et al., 1986; Cheng, 1989a–c; Sugar et al., 1991a, b; Chen et al., 1990a, b, 1992) on fluorescent probes have been focused on exploring the reorientational order, local wobbling diffusion rate, curvature-related lateral diffusion rate, and lateral diffusion rate of the lipids in the lipid membranes. The above physical parameters reflect the intermolecular dynamics or interactions of the host lipid membranes. On the other hand, information that is related with the internal motions, or intramolecular dynamics and interactions, within a single lipid has started to gain some attention recently (Melnick et al., 1981; Cheng et al., 1991; Vauhkonen et al., 1990; Sassaroli et al., 1993). The dual-chain pyrene-labeled dipyrenyl lipids represent a new class of fluorescent probes (Cheng et al., 1991; Eklund et al., 1992; Sassaroli et al., 1993) in investigating the structural dynamics of membranes. This new class of lipid probes has the distinct advantage of being able to probe the intramolecular dynamics of the acyl chains independent of the rotational and lateral mobilities of the whole lipid molecules in the membranes. Furthermore, by altering the length of the pyrene-labeled chains (Eklund et al., 1992), one can also examine the acyl chain dynamics of the lipid layer at different depths of the membranes.

Several studies (Vauhkonen et al., 1990; Eklund et al., 1992; Sassaroli et al., 1993) on using the steady-state excimer-to-monomer (E/M) intensity ratio of dipyrenyl lipids to probe the intramolecular dynamics and conformation of the lipid membranes have been reported. Our research group has also initiated several nanosecond-resolved studies (Cheng et al., 1991; Liu et al., 1993) in exploring the rates of excimer formation kinetics using dipyrenyl lipids of a fixed length in membranes. However, a systematic nanosecond-resolved study of using dipyrenyl lipids of different chain lengths in either isotropic solution or well defined lipid membranes has not been performed.

This study attempts to explore the intramolecular dynamics of the dipyrenyl lipids of different chain lengths by using frequency-domain fluorescence intensity decay technique, and by employing two different excited-state reaction models to analyze the fluorescence intensity decay data. The major

Received for publication 24 January 1994 and in final form 18 May 1994.
Address reprint requests to Dr. Kwan-Hon Cheng, Biophysics Laboratory, Department of Physics, Box 41051, Texas Tech University, Lubbock, TX 79409-1051. Tel.: 806-742-2992; Fax: 806-742-1182; E-mail: vckhc@ttacs.ttu.edu.

0006-3495/94/08/902/12 $2.00

goal of this study was to derive useful intramolecular dynamics information regarding the rotational mobility as well as the conformation of the lipophilic molecules in the lipid membranes within the nanosecond fluorescence time scale.

Selective information of the molecular dynamics of lipophilic molecules, e.g., dipyrenyl lipids used in this study, at different time scales will provide useful information in understanding the mechanism of lipid/protein interaction. For example, in calcium transport ATPase and probably other integral membrane proteins, concerted movements of several α-helices, also known as the anisotropic breathing mode, within the transmembrane region of the protein are believed to play a significant role in their biological functions and thermal stability in the cell membranes (Cheng et al., 1987; MacLennan, 1990; Lepock et al., 1990; Cheng and Lepock, 1992). Knowledge of how the lipid composition of the bilayer membranes effects and modulates the structural dynamics of the transmembrane portion of the protein at different locations of the membranes is required. In this study, the kinetic parameters of the intramolecular pyrene molecules of dipyrenyl lipids with different chain lengths provide site-selective molecular dynamics information of lipophilic molecules in the lipid bilayer membranes within the nanosecond time regime. Dipyrenyl lipids of different chain lengths were first studied in an isotropic liquid, pure ethanol, and then in well defined dimyristoylphosphatidylcholine (DMPC) lipid bilayer membranes. The differential interactions of cholesterol at different depths of the DMPC membranes were also examined. A brief description of the excited-state reaction models and the important assumptions of those models are also presented in this paper. Using an identical analytical procedure as in this paper, the results of the intramolecular dynamics of the dipyrenyl lipids in a binary lipid membranes system exhibiting composition-driven bilayer-to-nonbilayer phase transition are presented in a companion paper.

MATERIALS AND METHODS

Sample preparations

DMPC in chloroform was purchased from Avanti Polar Lipids (Birmingham, AL) and used without further purification. Cholesterol in dry powder was obtained from Kodak (Rochester, NY). No detectable fluorescence signal was found for all of the lipid samples in solutions or in lipid membranes. Single-chain pyrene-labeled phosphatidylcholine (PC) lipids, Py_nPC, and dual-chain pyrene-labeled PC, $Dipy_nPC$, with different chain lengths (n = 4, 6, 8, 10, and 12) were synthesized by methods described previously (Vauhkonen et al., 1990; Patel et al., 1979). Here Py_nPC is a diacyl PC that has a single planar pyrene molecule attached to the terminal methyl end of the *sn*-2-saturated acyl chain of n carbon long, and its *sn*-1 chain is a saturated chain of 16 carbon long. On the other hand, $Dipy_nPC$ is a diacyl PC lipid, but it has two pyrene molecules separately attached to both terminal methyl ends of two identical saturated chains (*sn*-1 and *sn*-2) of n carbon long.

Fig. 1 shows the dimensions of $Dipy_4PC$, $Dipy_{10}PC$, and DMPC. For simplicity, the lipids are depicted with their acyl chains in the all-*trans* configurations, and the polar headgroups are represented by ellipsoids. The regions of water bilayer membrane interface (W/B) and bilayer center (BC) are labeled. Note that the one methylene unit penetration difference of the *sn*-1 and *sn*-2 chains is based on a previous quantitative analysis of $Dipy_nPC$ in lipid membranes (Eklund et al., 1992). As shown in Fig. 1, the size of a pyrene molecule is similar to that of the membrane thickness. One might expect a rather strong perturbation of the membrane lattice around the intralipid pyrene moieties. However, if only a trace amount (0.1 mol%) of dipyrenyl lipids are present in the membranes, the collective properties of the membranes, such as phase transition temperature and enthalpy, will not be significantly altered. It is believed that the effect of the "bulky" dipyrenyl lipid molecules on the phase and physical properties of the membranes can be characterized by the ratio of the surface area covered by the dipyrenyl lipids to the total surface area of the membranes, rather than by the ratio of the pyrene size to the membrane thickness.

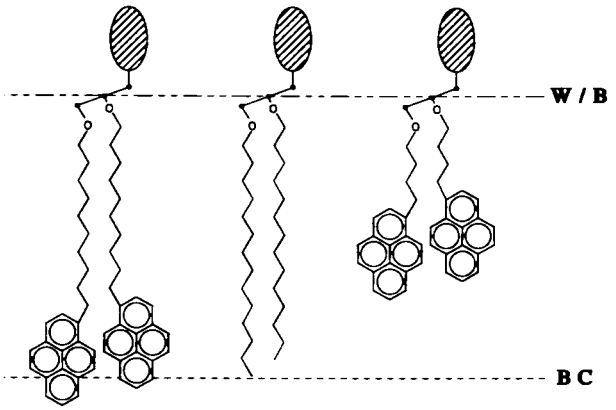

FIGURE 1 Schematic representation of the dimensions of $Dipy_{10}PC$ (*left*), DMPC (*middle*), and $Dipy_4PC$ (*right*) molecules. The lipids are depicted with their acyl chains in the all-*trans* configurations. The regions of water bilayer membrane interface and bilayer center are denoted by W/B and BC, respectively. The headgroups of the lipids are represented by shaded ellipsoids for simplicity.

For the fluorescence measurements in isotropic solution, the fluorescent lipids, Py_nPC and $Dipy_nPC$, were added to pure ethanol at a concentration of 0.2×10^{-6} M, whereas for the measurements in lipid bilayer membranes, these fluorescent lipids were added to DMPC, with or without 30 mol% cholesterol, in chloroform at the molar ratios of 0.05 and 0.1%, respectively. The mixtures were dried under nitrogen gas and kept under vacuum for at least 5 h. The dry lipid films were subsequently hydrated in an aqueous buffer (100 mM NaCl/10 mM TES/2 mM EDTA; pH 7.4) at 0°C under mild sonication for a few seconds. Thereafter, the suspensions were incubated at 0°C for 20 h in the dark to ensure proper hydration of the lipids. Upon further diluting, the lipid suspensions to less than 50 μg/ml, each sample was put into a 10 mm quartz cuvette. During the fluorescence measurements, the sample temperature was regulated by an external water-jet circulator and determined by inserting a microtip thermistor probe into the cuvette at ~5 mm above the light path.

Steady-state fluorescence spectral measurements

All steady-state spectral measurements were performed on either a GREG-200 fluorometer (ISS Inc., Champaign, IL) or a fast (millisecond-resolved) home-built fluorometer equipped with a Proximity Focused Intensified photodiode array IRY-700S Detector (Princeton Instrument Inc., Trenton, NJ) attached to a SPEX Minimate 1681 C spectrograph (SPEX Industries, Inc., Edison, NJ). Either a Liconix 4240NB cw He-Cd laser (Santa Clara, CA) with an output of 10 mW at 325 nm or a 1000 W Xenon Arc Lamp with the excitation wavelength selected by a monochromator at 325 nm was employed as the excitation source. The emission wavelength and spectral response of the detectors were calibrated using a standard mercury arc lamp and a fluorescent standard (tetraphenylbutadiene), respectively. The background from the solvent was always subtracted from the emission spectra of all of the samples. The spectral resolution of both instruments was better than 1 nm. Identical and reproducible spectra were obtained using either instrument.

Nanosecond-resolved frequency-domain fluorescence intensity decay measurements

All frequency-domain fluorescence intensity decay measurements were performed on a GREG-200 multifrequency cross-correlation fluorometer (ISS Inc., Champaign, IL) using a Liconix 4240NB cw He-Cd laser (Santa Clara, CA) with an output of 10 mW at 325 nm as the excitation source. The operational principle of this fluorometer has been described in detail elsewhere (Lakowicz, 1983; Gratton et al., 1984). Briefly, for samples containing Dipy$_n$PC, modulated fluorescence signals at 392 and 475 nm, which correspond to the fluorescence intensity peaks of the monomer and excimer emissions of pyrene derivatives, respectively, were measured through a monochromator (slit width = 2.0 nm). Specifically, phase delays and demodulation ratios of the fluorescence signal from each sample as compared with that from a standard solution of 1,4-bis[2-(5-phenyl-oxazolyl)]benzene in ethanol (fluorescence lifetime = 1.34 ns) were measured at different modulation frequencies ranging from 100 kHz to 50 MHz. For the samples containing Py$_n$PC, fluorescence signals at the monomer emission (392 nm) were detected and similar phase delays and demodulation ratios were acquired. Because the light exiting from the pockels cell (electro-optical device) is vertically polarized, a polarizer with its polarization axis set at 35° with respect to the vertical was placed in the excitation beam to eliminate the contribution of the rotational diffusion effect of the sample to the measurements (Cheng, 1989a; Sugar et al., 1991a).

The method of calculating the single monomer fluorescence lifetime of Py$_n$PC from the frequency-domain fluorescence intensity decay data has been described previously (Lakowicz, 1983; Gratton et al., 1984). The inverse of the monomer fluorescence lifetime gives the rate constant K_m, which is defined as the rate of decay of the excited monomer back to the ground state in the absence of excimer formation. As discussed later, this rate constant is required in both the 2- and 3-state fits.

The following sections outline the mathematical models used for calculating the kinetic parameters of Dipy$_n$PC from the dual-channel frequency-domain fluorescence intensity decay data at 392 and 475 nm.

Mathematical models for analyzing the kinetic parameters of dipyrenyl lipids

The general mathematical approach for analyzing the frequency-domain monomer and excimer fluorescence intensity decay data of pyrene derivatives has been described in detail previously (Sugar, 1991; Sugar et al., 1991a, b). Only a brief summary of the theoretical models and equations used in this study is presented below.

Upon excitation by an extremely short light pulse, the fluorescent states of the pyrene derivatives can be characterized by a state vector $\mathbf{X} = [X_1, X_2, \cdots, X_n]$, where X_i is the proportion of the excited pyrene derivatives in the ith excited state and n is the total number of excited states. Assume that the rates of fluorescence decay processes of the excited states can be described by a set of first-order linear differential equations (Sugar, 1991) of the form

$$\frac{dX_i}{dt} = \sum_{j=1}^{n} T_{ij}X_j, \tag{1}$$

where $\mathbf{T}$ is defined as the transfer matrix. All of the kinetic parameters of the decay processes are contained in this $\mathbf{T}$ matrix. Upon establishing a kinetic model and appropriate initial conditions, i.e., $\mathbf{X}$ at time $t = 0$, Eq. 1 can be solved and the time-dependent fluorescence emission of the pyrene derivatives $f(t, \lambda)$ can be expressed in terms of $\mathbf{X}(t)$ in the following form:

$$f(t, \lambda) = \sum_{j=1}^{n} S_j(\lambda)X_j(t), \tag{2}$$

where λ and $S_j(\lambda)$ are the emission wavelength and the species-associated spectrum of the jth excited species.

For the case of frequency-domain measurements, the intensity of the excitation light is in the form of a sinusoidally modulated form, and a complex demodulation function $m_E(\omega, \lambda)$ can be measured. Here ω represents the angular modulation frequency. Specifically, the absolute value and phase angle of $m_E(\omega, \lambda)$ are equivalent to the demodulation level and phase delay of the fluorescence signal collected at the wavelength λ. It has been shown (Sugar, 1991) that $m_E(\omega, \lambda)$ is associated with $\tilde{f}(\omega, \lambda)$, the fourier transform of $f(\omega, \lambda)$. In addition, the experimental parameter, steady- state excimer-to-monomer fluorescence intensity ratio (E/M) is identical to $\tilde{f}(0, \lambda_D)/\tilde{f}(0, \lambda_M)$, where λ_D and λ_M are the excimer and monomer emission wavelengths, respectively.

Based on a given kinetic model (e.g., 2-state or 3-state model in our case), the theoretical values of the state vector $\tilde{X}(\omega)$, fourier transform of $X(t)$, can be expressed in terms of the kinetic parameters of the pyrene derivatives. Consequently the theoretical values of $m_E(\omega, \lambda)$ can also be determined (Sugar, 1991). Therefore, by measuring the experimental $m_E(\omega, \lambda)$, the kinetic parameters of the pyrene derivatives can then be calculated by comparing with the theoretical $m_E(\omega, \lambda)$ using a nonlinear least-squares procedure. In the following sections, we summarize the kinetic models, 2-state and 3-state, that are used to calculate the theoretical $m_E(\omega, \lambda)$.

2-State kinetic model ($X = [\bar{M}^*, \bar{D}^*]$) of dipyrenyl lipids

The 2-state model describes the photophysics of dipyrenyl lipids in membranes. The model is rather similar to the Birks model (Birks et al., 1963), which describes the photophysical behavior of pyrene in solution. The two excited species in our 2-state model are $\bar{M}^*$ (X_1) and $\bar{D}^*$ (X_2) as shown in Fig. 2. In the case of $\bar{M}^*$ state, one of the pyrene moieties of the dipyrenyl lipid is excited, whereas $\bar{D}^*$ state refers to the intramolecular excimer formation of the pyrene moieties in the dipyrenyl lipid molecule. The model neglects intermolecular excimer formations because of the very low (0.1%) mole fraction of dipyrenyl lipid in the membranes. We also neglect the presence of doubly excited dipyrenyl lipid molecules because of the low intensity of the excitation. Thus, the kinetic scheme of our model agrees with that of the Birks model, although in the Birks model excimer (D^*) forms from the collision of any excited pyrene M^* and ground state pyrene M, whereas in our model the excimer formation is an intramolecular excited-state reaction. Bars are used to differentiate the states of our 2-state model

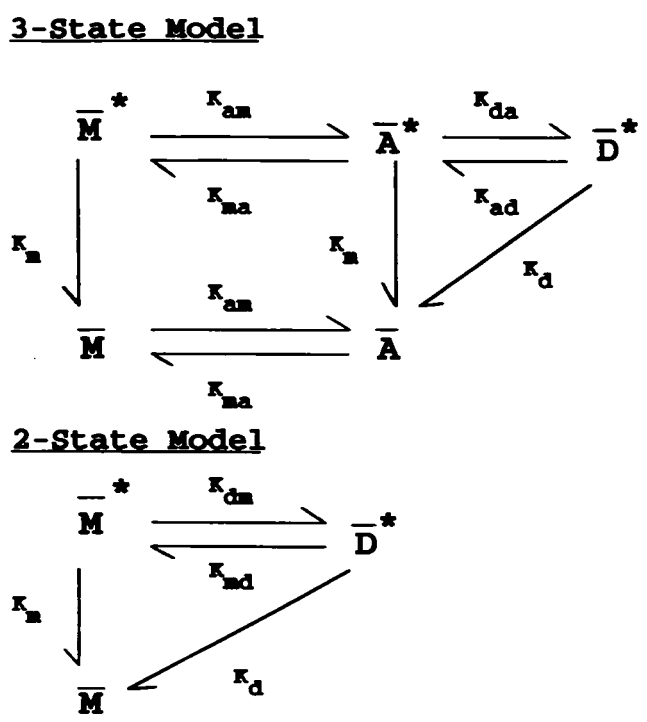

FIGURE 2 Schematic diagrams of the 2- and 3-state kinetic models of dipyrenyl lipids. The notations are described in Materials and Methods.

from the states of the Birks model. The association and dissociation rate constants for the excimer are given by K_{dm} and K_{md}, respectively. The decay rate constants of $\bar{M}^*$ and $\bar{D}^*$ back to their ground states are given by K_m and K_d, respectively. The explicit forms of $\bar{X}_1(\omega)$, $\bar{X}_2(\omega)$, $m_E(\omega, \lambda_M)$, and $m_E(\omega, \lambda_D)$ for the 2-state model are given in the appendix.

3-State kinetic model ($X = [\bar{M}^*, \bar{A}^*, \bar{D}^*]$) of dipyrenyl lipids

The 3-state kinetic model suggests the existence of three excited species of pyrene derivatives, $\bar{M}^*$ (X_1), aggregated state $\bar{A}^*$ (X_2), and $\bar{D}^*$ (X_3). The excited-state reaction involves a 2-step process as shown in Fig. 2. In both $\bar{M}^*$ and $\bar{A}^*$ states, one of the pyrene moieties of dipyrenyl lipid molecule is excited. In the aggregated state $\bar{A}^*$, the two pyrene moieties are in close apposition and an elementary change in the relative orientation of the pyrene moieties might result in intramolecular excimer $\bar{D}^*$ formation. Because two steps are involved in excited-state reaction, four rate constants are required to describe the formation of $\bar{M}^*$ from $\bar{D}^*$. These constants are the association and dissociation rate constants for the $\bar{A}^*$ state, i.e., K_{am} and K_{ma}, respectively, and the association and dissociation rate constants for the $\bar{D}^*$ state, i.e., K_{da} and K_{ad}, respectively. Note that this 3-state model predicts (Sugar et al., 1991b) that the ground state $\bar{A}$ can be directly excited to form the excited $\bar{A}$ state, $\bar{A}^*$. In addition, the rate constants governing the association and dissociation kinetics for the $\bar{A}$ state are assumed to be equivalent to those from the $\bar{A}^*$ as shown in Fig. 2 (Sugar et al., 1991b; Liu et al., 1993). On the basis of the above assumptions, the ratio of the initial values of X_1 and X_2 is then equal to K_{am}/K_{ma}. The explicit forms of $\bar{X}_1(\omega)$, $\bar{X}_2(\omega)$, $\bar{X}_3(\omega)$, $m_E(\omega, \lambda_M)$ and $m_E(\omega, \lambda_D)$ are given in the appendix.

Data analysis

Several rate constants are involved in the theoretical excited-state reaction models. As shown in the reaction scheme (Fig. 2), these rate constants are (K_{dm}, K_{md}, K_d, and K_m) and (K_{da}, K_{ad}, K_{am}, K_{ma}, K_d, and K_m) for the 2- and 3-state models, respectively. In addition, the value of K_{fd}/K_{fm}, which is defined as the ratio of the radiative decay rate constant of the excimer and that of the monomer, is required to calculate the theoretical E/M ratio for both the 2- and 3-state models (Sugar et al., 1991a, b). Hence, K_d, K_m, and K_{fd}/K_{fm} are common to both kinetic models. As shown in Fig. 2, these parameters are used to describe the photodecay behavior of the excited monomer and excimer states to the same ground state, and should be independent of the excited-state reactions of the pyrene derivatives. In this present study, K_m can be determined independently from the measured fluorescence lifetime of the single pyrene-labeled Py$_n$PC. Its value of K_m was found to be 4.3×10^7 s^{-1} in ethanol and $0.7–1.0 \times 10^7$ s^{-1} in lipid bilayer membranes, and is independent of the chain length of Py$_n$PC. Now K_{fd}/K_{fm} is a photochemical parameter of the pyrene derivatives. Using either the 2- or 3-state model, its value was found to be around 0.7–1.5, similar to several previous studies on the same pyrene derivatives (Sugar et al., 1991a, b). For simplicity, its value was fixed at 1.0 for all of the analysis presented in this study. Upon fixing the values of the K_m and K_{fd}/K_{fm}, the fitting parameters for the 2- and 3-state are reduced to (K_{dm}, K_{md}, and K_d) and (K_{da}, K_{ad}, K_{am}, K_{ma}, and K_d), respectively.

A nonlinear least-squares search procedure utilizing the modified Gauss-Newton search method (Johnson, 1983) for minimizing the value of χ^2 was employed to determine the above described rate parameters as described in the 2- and 3-state models. The raw frequency-domain data were in the forms of phase delay and demodulation as a function modulation frequency at two different wavelengths (392 and 475 nm). These data represented four dependent variables and one independent variable (angular frequency). Because the theoretical models are expressed in the forms of complex demodulation factors $m_E(\omega, \lambda_M)$ and $m_E(\omega, \lambda_D)$, these raw frequency-domain data were further transformed into four different dependent variables, namely $\mathrm{Re}(m_E(\omega, \lambda_M))$, $\mathrm{Im}(m_E(\omega, \lambda_M))$, $(\mathrm{E/M}) \cdot \mathrm{Re}(m_E(\omega, \lambda_D))$, and $(\mathrm{E/M}) \cdot \mathrm{Im}(m_E(\omega, \lambda_D))$. Note that $m_E(\omega, \lambda_D)$ was weighted by the E/M ratio so as to take into account of the fluorescence intensity differences measured at the monomer and excimer emission channels. The above four different variables as a function of angular frequency constituted the data set for the nonlinear parameter estimation. Here, the chi square, χ^2, is defined as the sum of the squares of deviations between the observed and expected values of the four variables over all the modulation frequencies divided by the degree of freedom. Each deviation in the above sum was further divided by the experimental uncertainty, which was determined using the standard method of error propagation (Sugar et al., 1991b). In some cases, the nonlinear parameter estimation procedures were also performed on the original raw frequency-domain data, i.e., phase delay and demodulation. In those cases, the values of K_{fd}/K_{fm} were not required. Similar fitting results were obtained as compared with fitting using the complex modulation factors. A detailed description of the frequency-domain fitting procedure and the estimation of the confidence limits has been described elsewhere (Johnson, 1983; Davenport et al., 1986; Ameloot et al., 1986; Cheng, 1989a; Sugar et al., 1991a, b; Liu et al., 1993).

Proposed relationships of the kinetic parameters and conformational dynamics of dipy$_n$PC

Information pertaining to the conformational dynamics of the intramolecular pyrene moieties can be derived from the kinetic parameters calculated from the theoretical kinetic models.

For the 2-state model, the K_{dm} is associated with the relative approaching rate of the pyrene moiety with respect to its neighbor within the Dipy$_n$PC lipid. The above rate should be controlled by both the lateral and rotational mobilities of the pyrene molecules at a defined depth of the lipid membranes (see Fig. 1). The reverse rate constant, K_{md}, which is the rate of dissociation of the dimer, should be closely related with the intrinsic photochemical nature of the dimer.

For the 3-state model, the lateral and rotational mobility contributions to the excimer formation can be separated. Here, K_{da} is controlled solely by the rotational mobility of the pyrene molecule, because the two pyrenes are already in close apposition in the $\bar{A}^*$ state (see Fig. 2). The K_{ad} should be identical to K_{md}, both referring to the dissociation rate of the dimer. The forward and reverse rate constants, K_{am} and K_{ma}, are controlled by the lateral mobility of the acyl chains. Furthermore, the ratio K_{am}/K_{ma} is the equilibrium constant of the $\bar{M} \rightleftharpoons \bar{A}$ reaction as discussed in the previous section.

RESULTS

Steady-state fluorescence spectral measurements of Py$_n$PC and Dipy$_n$PC in ethanol and lipid bilayer membranes

Corrected steady-state fluorescence spectra were measured for Py$_n$PC and Dipy$_n$PC in 100% ethanol and in DMPC lipid bilayer membranes. Typical fluorescence emission spectra of pyrene derivatives have been presented elsewhere (Melnick et al., 1981; Chong and Thompson, 1985) and, therefore, are not shown. At 0.2×10^{-6} M in ethanol and 0.1 mol% in DMPC (with or without 30 mol% cholesterol), no excimer emission was detected for Py$_n$PC, but strong and broad excimer emission centered at around 475 nm was found for Dipy$_n$PC. Both Py$_n$PC and Dipy$_n$PC exhibited typical vibronic bands of the pyrene monomer emission (Melnick et al., 1981). From the Dipy$_n$PC spectra, the values of the steady-state excimer-to-monomer intensity (E/M) ratio, i.e., intensity at 475 nm divided by that at 392 nm, were calculated. Using a simple titration method (Cheng et al., 1991), the E/M ratios of Dipy$_n$PC in either pure solvent or in lipid membranes were found to be insensitive to the relative concentrations of the probes within the concentration ranges described above. This observation indicated that the fluores-

cence properties reported in this study were mainly intramolecular events.

Fig. 3 shows the variation of E/M ratio of Dipy$_n$PC in ethanol as a function of chain length n and at a fixed temperature of 20°C. It was observed that the E/M ratio of Dipy$_n$PC declined steadily from n = 4–8 but remained essentially constant for higher values of n.

Fig. 4 shows the temperature dependence of E/M ratios of Dipy$_4$PC and Dipy$_{10}$PC in lipid bilayer membranes of DMPC in the absence and presence of 30 mol% cholesterol. In the absence of cholesterol, the E/M ratio increased steadily with temperature from 0 to ~23°C for Dipy$_4$PC but less so for Dipy$_{10}$PC. An abrupt increase in the E/M ratio was found for both Dipy$_4$PC and Dipy$_{10}$PC at ~23°C, the known gel (L_β)-to-liquid crystalline (L_α) phase transition of DMPC. As the temperature increased further to 40°C, the E/M ratios for both Dipy$_4$PC and Dipy$_{10}$PC increased steadily again with temperature. In the presence of cholesterol, the values of E/M ratio changed significantly for Dipy$_{10}$PC, but not for Dipy$_4$PC, when compared with those in the absence of cholesterol. Here the E/M ratios in the presence of cholesterol increased by two- to threefold for Dipy$_{10}$PC at all temperatures (0–40°C). At the temperature range of 25–35°C, only a slight decrease in the E/M ratio was observed for Dipy$_4$PC in the presence of cholesterol.

Frequency-domain fluorescence intensity decay measurements of Py$_n$PC and Dipy$_n$PC in ethanol and lipid bilayer membranes

Phase delays and demodulations of the fluorescence emission of Py$_n$PC at 392 nm, and Dipy$_n$PC at both 392 and 475 nm were measured as a function of modulation frequency ranging from 0.1 to 50 MHz. As described in the Materials and Methods, the values of K_m of monomeric pyrene derivatives in ethanol and lipid membranes were determined from the frequency-domain data of Py$_n$PC. The frequency-domain data of Dipy$_n$PC were further transformed into the complex forms, Re($m_E(\omega, \lambda_M)$), Im($m_E(\omega, \lambda_M)$), (E/M) · Re($m_E(\omega, \lambda_D)$), and (E/M) · Im($m_E(\omega, \lambda_D)$), for different modulation frequencies and at two emission channels, λ_M (392 nm) and λ_D (475 nm). For simplicity, $m_E(\omega, \lambda_M)$ and $m_E(\omega, \lambda_D)$ were expressed as m_M and m_D, respectively, later on in the presentation. Fig. 5 shows a typical example of the transformed frequency-domain data, Re(m_M) and Im(m_M) in panel *A*; and (E/M) · Re(m_D) and (E/M) · Im(m_D) in panel *B*, obtained from Dipy$_{10}$PC in DMPC at 32°C. In the complex space plots, each point represents one single angular modulation frequency ω. As ω increased, the data point migrated from the lower right hand corner towards the upper left hand corner. The uncertainties of the data points were also presented. Because of the involvement of E/M in the plot of m_D, the uncertainties for the data point of m_D were usually larger than those of m_M as demonstrated in Fig. 5.

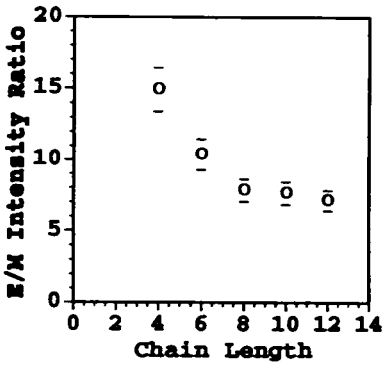

FIGURE 3 A plot of corrected E/M intensity ratio as a function of the chain length (n) of Dipy$_n$PC in ethanol at 20°C. The bars indicate uncertainties in the measurements. The concentration of Dipy$_n$PC was 0.2×10^{-6} M.

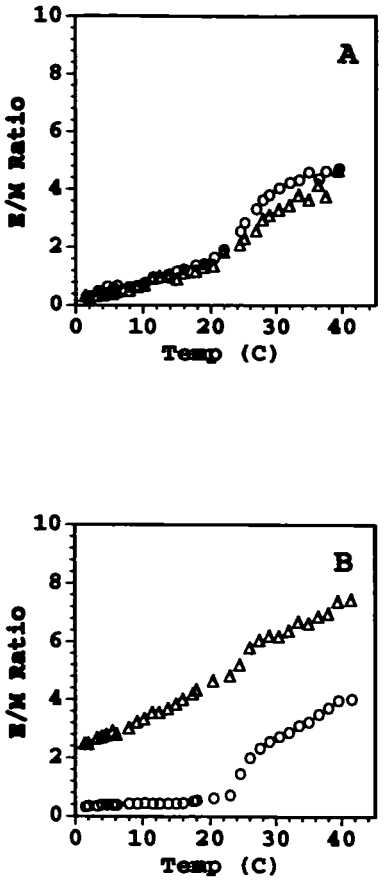

FIGURE 4 Plots of the corrected E/M intensity ratio of Dipy$_4$PC (*A*) and Dipy$_{10}$PC (*B*) in DMPC, in the absence (○) and presence (△) of 30 mol% cholesterol, as a function of temperature. The usual uncertainty of the measurement was roughly the size of the symbol and is not shown for simplicity. The concentration of either Dipy$_4$PC or Dipy$_{10}$PC in the host lipid membranes was 0.1 mol%.

Calculations of the kinetic parameters of Dipy$_n$PC in ethanol and lipid bilayer membranes

Both the 2- and 3-state models were employed to fit the frequency-domain data. It is important to mention that the

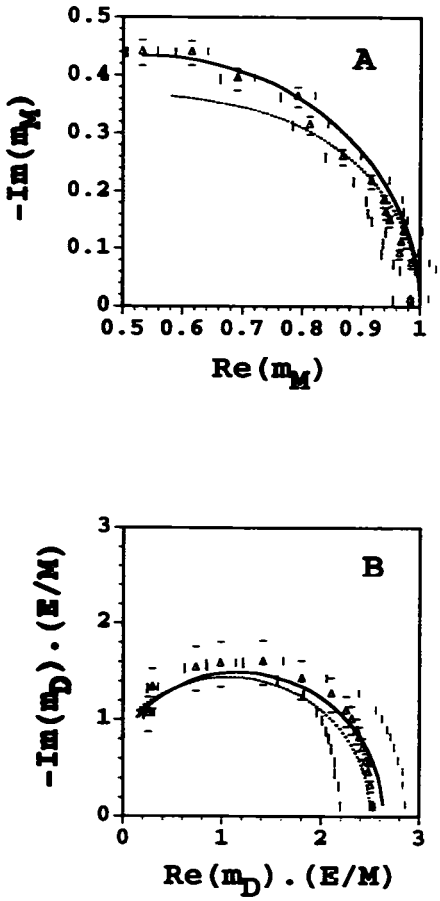

FIGURE 5 (*A*) A plot of the negative of the imaginary part (Im) of the complex modulation factor for the monomer emission (m_M) versus the real part (Re) of m_M for $Dipy_{10}PC$ in DMPC membranes at 32°C. (*B*) A plot of the product of the Im part of the complex modulation for the excimer emission (m_D) and E/M ratio versus the product of Re part of m_D and E/M for $Dipy_{10}PC$ in DMPC membranes at 32°C. The molar concentration of $Dipy_{10}PC$ in DMPC was 0.1%. The bars indicate uncertainties of the data. The dotted and solid lines represent the theoretical curves generated by the fitting using the 2-state and 3-state models, respectively. The fitted parameters (K_{dm}, K_{md}, and K_d) for the 2-state and (K_{da}, K_{ad}, K_{am}, K_{ma}, and K_d) for the 3-state models are shown in Table 2.

TABLE 1 Comparisons of the fitting parameters (K_{dm}, K_{md}, K_d) and (K_{da}, K_{ad}, K_{am}, K_{ma}, K_d) from the 2- and 3-state fits, respectively, for $Dipy_{10}PC$ in ethanol at 20°C

Fitting parameters	2-State kinetic model	3-State kinetic model		
K_{da} or K_{dm} ($10^7 s^{-1}$)	32.8 (27.2, 38.1)	115 (88.1, 161)	129 (101, 178)	127 (94.1, 178)
K_{ad} or K_{md} ($10^7 s^{-1}$)	0.77 (0.46, 1.14)	0.59 (0.23, 1.25)	0.81 (0.41, 1.49)	0.77
K_{am} ($10^7 s^{-1}$)		14.5 (11.6, 19.5)	15.5 (12.7, 20.2)	15.3 (13.3, 17.1)
K_{ma} ($10^7 s^{-1}$)		4.96 (2.71, 9.03)	5.64 (3.19, 9.91)	5.47 (3.01, 7.85)
K_d ($10^7 s^{-1}$)	3.98 (3.46, 4.58)	4.34 (3.92, 4.76)	3.98	3.98
χ^2	5.73	3.01	3.03	3.02
K_{am}/K_{ma}		2.92 (1.29, 7.20)	2.75 (1.28, 6.33)	2.79 (1.69, 5.68)

Values in parentheses are confidence limits, whereas those without parentheses are fixed during the fits. The chisquares χ^2 of each fit is also shown.

TABLE 2 Comparisons of the fitting parameters (K_{dm}, K_{md}, K_d) and (K_{da}, K_{ad}, K_{am}, K_{ma}, K_d) from the 2- and 3-state fits, respectively, for $Dipy_{10}PC$ in DMPC at 32°C

Fitting parameters	2-State kinetic model	3-State kinetic model		
K_{da} or K_{dm} ($10^7 s^{-1}$)	5.98 (5.44, 6.59)	15.3 (12.8, 19.1)	16.4 (13.6, 20.5)	24.9 (20.1, 30.7)
K_{ad} or K_{md} ($10^7 s^{-1}$)	0.71 (0.59, 0.87)	0.34 (0.20, 0.56)	0.40 (0.25, 0.60)	0.71
K_{am} ($10^7 s^{-1}$)		2.22 (1.89, 2.72)	2.31 (1.99, 2.78)	2.86 (2.69, 3.03)
K_{ma} ($10^7 s^{-1}$)		1.12 (0.75, 1.69)	1.22 (0.83, 1.80)	2.26 (1.97, 2.54)
K_d ($10^7 s^{-1}$)	1.64 (1.56, 1.73)	1.61 (1.56, 1.67)	1.64	1.64
χ^2	0.93	0.28	0.28	0.28
K_{am}/K_{ma}		1.98 (1.12, 3.62)	1.89 (1.11, 3.39)	1.27 (1.06, 1.54)

Values in parentheses are confidence limits, whereas those without parentheses are fixed during the fits. The chisquares χ^2 of each fit is also shown.

analysis of the kinetic parameters in this study involves simultaneous considerations of the fluorescence decays of the dipyrenyl lipids at two distinctively separated emissions, monomer and excimer. In addition, the independently measured E/M ratio and K_m were also used in all the fittings (see Materials and Methods).

Tables 1 and 2 show the typical values of the fitted parameters, i.e., (K_{dm}, K_{md}, and K_d) for the 2-state model and (K_{da}, K_{ad}, K_{am}, K_{ma}, and K_d) for the 3-state model, for $Dipy_{10}PC$ in ethanol at 20°C and in DMPC at 32°C, respectively. For the case of 3-state model, confined fits, i.e., keeping one or two parameters fixed during the fitting procedures, are also shown. The free parameters for these confined fits, were (K_{da}, K_{ad}, K_{am}, and K_{ma}) and (K_{da}, K_{am}, and K_{ma}). The values of the fixed parameters in those confined fits were based on those obtained from the 2-state fits. As shown in both Tables 1 and 2, good improvements in the chi square of the 3-state fit over those of the 2-state fit were observed. In addition, the confidence limits of the fitted parameters from the confined fits were more narrower than those from the free fits, particular for the K_{am} and K_{ma}. No significant differences in the chi squares were found for the confined 3-state fits as compared with those for the free 3-state fit. In agreement with the chi square values, the theoretical curves generated by the 3-state model fitted the complex frequency-domain data better than did those from the 2-state model, as shown in Fig. 5.

The identifiability or uniqueness nature (Johnson, 1983; Davenport et al., 1986; Ameloot et al., 1986) of the fitted parameters from the 2- and 3-state fits has been carefully

examined by monitoring the cross-correlation matrix elements of the fitting parameters. The upper and lower limits of all the fitted parameters were determined by a searching procedure using an F-statistics with a 65% confidence probability (Johnson, 1983). These limits provide a better idea of the possible ranges of the fitting parameters and suitable for cross-comparisons among different samples than do the conventional fitting uncertainties derived from the diagonal elements of the error matrix (Johnson, 1983; Ameloot et al., 1986). For the case of Dipy$_n$PC in ethanol, all the fitting parameters calculated from the 2- and 3-state fits were unique and converged properly during the nonlinear chi square minimization procedures. For Dipy$_4$PC and Dipy$_{10}$PC in lipid membranes, the fitting parameters calculated from the 2-state and confined 3-state fits (K_{da}, K_{aa}, and K_{ma}) were properly converged. However, the fitting parameters calculated from free 3-state fits (K_{ad}, K_{md}, K_{aa}, K_{ma}, and K_d) with five parameters were not always unique, particularly for Dipy$_4$PC at most temperatures and Dipy$_{10}$PC at low temperatures. Examinations of the correlation matrix in those conditions revealed that the parameters K_{ad} and K_{aa} were closely related and could not be varied independently. Because of the intrinsic identifiability problem in some conditions, fitting parameters obtained from confined 3-state fits were compared among different samples.

The chain-length (n) dependence of the kinetic parameters of Dipy$_n$PC in ethanol was examined. Here 2-state model and the confined 3-state model were used to analyze the data, and the fitted parameters were (K_{dm}, K_{md}, and K_d) and (K_{da}, K_{aa}, and K_{ma}), respectively. Figs. 6 and 7 show those kinetic parameters of Dipy$_n$PC as a function of n. The confidence limits for each parameter are also shown in all of the plots. For the 2-state fit, the values of K_{dm} declined progressively with increasing chain length, whereas K_{md} and K_d declined only slightly with increasing chain length. For the 3-state fits, K_{da} and K_{aa} decreased with increasing chain length. On the other hand, K_{ma} increased slightly with increasing chain length. Despite large uncertainties, the ratio of K_{aa}/K_{ma} appeared to decline progressively with increasing chain length as shown in Fig. 7 *C*. To determine the relative goodness of fits of the 3-state model as compared with those of the 2-state model for different chain lengths, the ratio of the chi square for the 3-state model with that for the 2-state model, or chi square ratio, was plotted as a function of the chain length (n) of Dipy$_n$PC and is shown Fig. 7 *D*. The chi square ratios for the free and confined fits for the 3-state models are shown. No significant changes in the chi square ratios were found among all the 3-state fits for each chain length, except for $n = 12$ in which the free 5-parameter fit was only slightly better than the confined fits. Interestingly, the chi square ratio was found to decrease significantly with increasing chain length.

The kinetic parameters calculated from the 2-state model for Dipy$_4$PC and Dipy$_{10}$PC in DMPC at different temperatures are shown in Figs. 8 and 9, respectively. In the absence of cholesterol, for both Dipy$_4$PC and Dipy$_{10}$PC, K_{dm} increased and K_{md} decreased with temperature, and abrupt changes, or transitions, were observed at the known L_β-L_α transition at ~23°C. On the other hand, K_d declined slightly with temperature before the phase transition and increased abruptly after the phase transition. By comparing the kinetic parameters of Dipy$_4$PC with those of Dipy$_{10}$PC at all temperatures (0–35°C), it was observed that K_{dm} of Dipy$_4$PC was larger than that of Dipy$_{10}$PC, K_{md} of Dipy$_{10}$PC was smaller than that of Dipy$_4$PC, and K_d was essentially the same for both Dipy$_4$PC and Dipy$_{10}$PC. The kinetic parameters calculated from the 2-state model for Dipy$_4$PC and Dipy$_{10}$PC in DMPC/Cholesterol membranes are also shown in Figs. 8 and 9, respectively. For Dipy$_4$PC, the values of K_{dm} and K_d were essentially unaltered by cholesterol at all temperatures, whereas significant increases in the values of K_{md} were noticed in the presence of cholesterol, especially in the gel phase. For Dipy$_{10}$PC, K_{dm} increased drastically by three- to fivefold and K_{md} decreased by two- to threefold in the

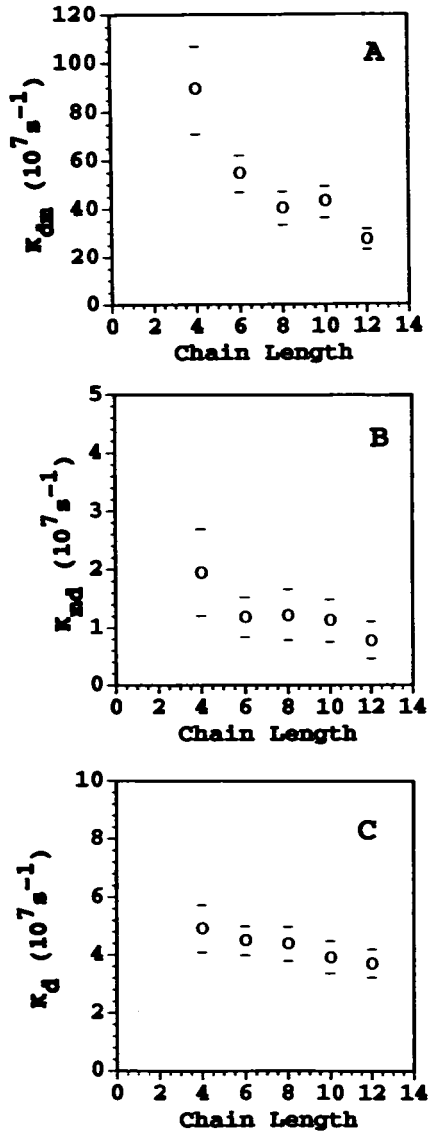

FIGURE 6 Plots of the fitted parameters, K_{dm} (*A*), K_{md} (*B*), and K_d (*C*), generated from the 2-state model as a function of chain length (n) of Dipy$_n$PC in ethanol at 20°C. The concentration of Dipy$_{10}$PC was 0.2×10^{-6} M. The bars indicate the confidence limits of the fitting.

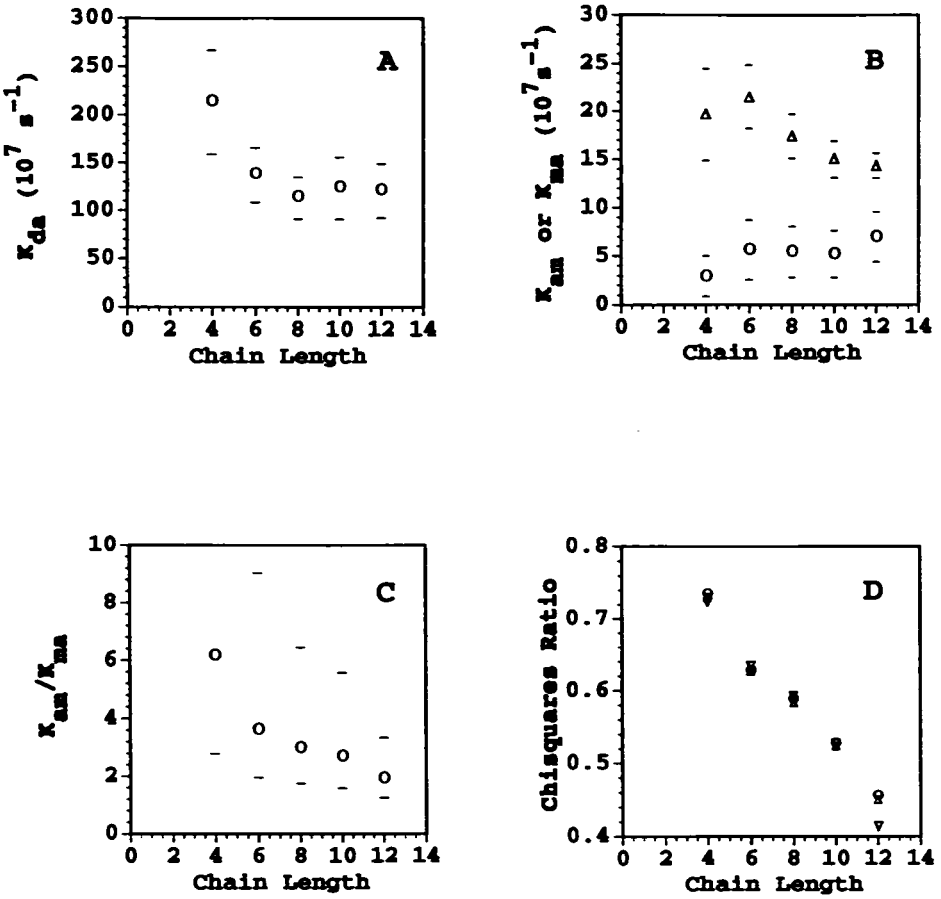

FIGURE 7 Plots of the fitted parameters, K_{da} (*A*), K_{am}, and K_{ma} (*B*) and K_{am}/K_{ma} (*C*), generated from the 3-state model as a function of the chain length (n) of Dipy$_n$PC in ethanol at 20°C. The above values were obtained by fixing the values of K_{ad} and K_d during the fitting. These values were identical to those obtained from the 2-state fits (see Materials and Methods). The concentration of Dipy$_{10}$PC was 0.2×10^{-6} M. A plot of the value of the ratio of chi squares from the 3-state fit to that from the 2-state fit, chi square ratio, as a function of the chain length (n) of Dipy$_n$PC is shown in *D*. The chi square ratios that involve different numbers of fitting parameters, (K_{da}, K_{ad}, K_{am}, K_{ma}, and K_d), (K_{da}, K_{ad}, K_{am}, K_{ma}) and (K_{da}, K_{am}, K_{ma}), are represented by ▽, △, and ○, respectively.

presence of cholesterol. Comparatively, K_d increased only slightly in the presence of cholesterol.

The kinetic parameters calculated from the 3-state model for Dipy$_4$PC and Dipy$_{10}$PC in DMPC and DMPC/cholesterol membranes at different temperatures are shown in Tables 3 and 4, respectively. The confined 3-state fits with three parameters (K_{da}, K_{am}, and K_{ma}) were used. In the absence of cholesterol, for Dipy$_4$PC, K_{da} increased by threefold after the L_β-L_α transition of DMPC, whereas no changes were observed for K_{am}/K_{ma}. For Dipy$_{10}$PC, K_{da} increased by sixfold and K_{am}/K_{ma} decreased by fivefold after the L_β-L_α transition of DMPC. The kinetic parameters of Dipy$_4$PC and Dipy$_{10}$PC in DMPC/Cholesterol membranes are also shown in Tables 3 and 4, respectively. For Dipy$_4$PC, a sixfold increase in K_{da} and a 50% decrease in K_{am}/K_{ma} were observed relative to the cholesterol free case at 15°C, i.e., at the L_β phase of DMPC, whereas no changes in either K_{da} or K_{am}/K_{ma} were found at 25 and 32°C, i.e., L_α phase of DMPC. For Dipy$_{10}$PC, a sixfold increase in K_{da} and a 10-fold increase in K_{am}/K_{ma} were found in the presence of cholesterol at 15°C. Similar trends were also noticed at higher temperatures, i.e., 25 and 32°C. The chi square of the 3-state, as well as the 2-state, fits is also shown in Tables 3 and 4. Based on the relative values of these chi square, it was concluded that the 3-state model provided a significantly better ($p < 0.05$) fit than did the 2-state model for Dipy$_{10}$PC at 25 and 32°C, whereas the 3-state model failed to provide a significantly better fit than did the 2-state model for Dipy4PC at all temperatures and Dipy$_{10}$PC at 15°C.

DISCUSSIONS

In this study, the relative conformation and rotational mobility of the intramolecular pyrene moieties in dipyrenyl lipids of different lengths have been investigated in solution as well as in well defined lipid bilayer membranes. Using two different excited-state reaction models, kinetic parameters of the pyrene moieties were calculated from the frequency-domain fluorescence intensity decay data collected at both monomer (392 nm) and excimer (475 nm) emission channels. An independent experimental parameter, E/M ratio, was used to link the two fluorescence emission data during the data fitting procedures (Sugar, 1991; Sugar et al., 1991a, b).

As for any molecular dynamics investigations, physical models and data fittings are necessary to extract meaningful information from the raw experimental data. Here, the kinetic parameters of the excited state reactions of dipyrenyl lipids were calculated. The 2-state model assumes that the excited state reaction is a 1-step process, whereas the 3-state model assumes a 2-step process and requires the existence of an intermediate reaction complex, aggregated state. Only the

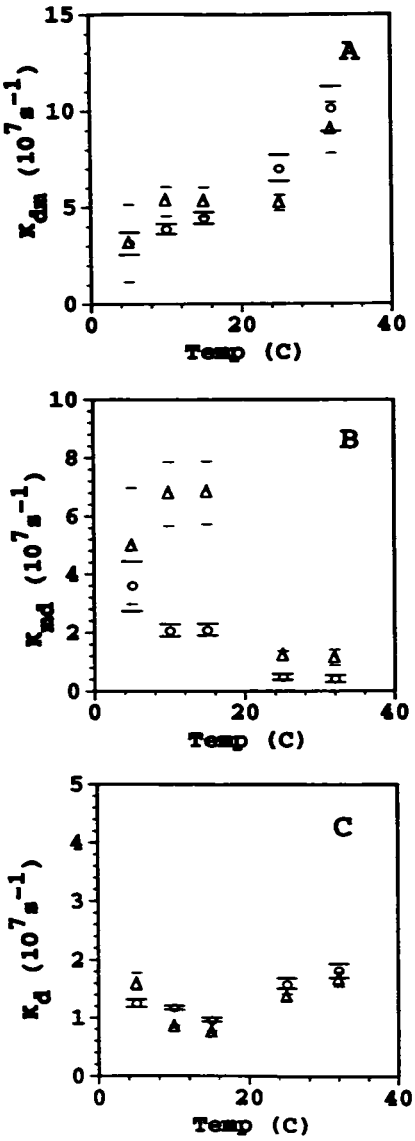

FIGURE 8 Plots of the fitted parameters, K_{dm} (*A*), K_{md} (*B*) and K_d (*C*), generated from the 2-state model as a function of temperature for $Dipy_4PC$ in DMPC, in the absence (○) and presence (△) of 30 mol% cholesterol. The concentration of $Dipy_4PC$ was 0.1 mol%. The bars indicate the confidence limits of the fittings.

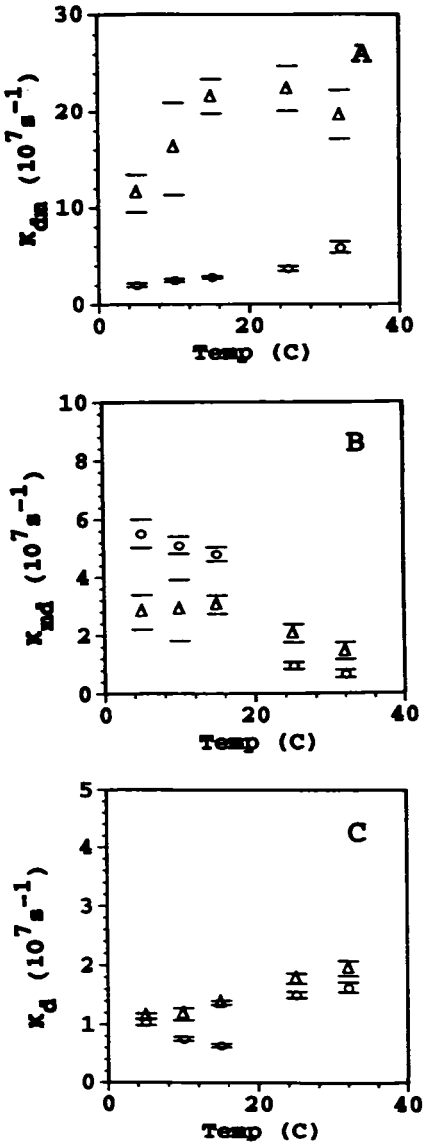

FIGURE 9 Plots of the fitted parameters, K_{dm} (*A*), K_{md} (*B*), and K_d (*C*), generated from the 2-state model as a function of temperature for $Dipy_{10}PC$ in DMPC, in the absence (○) and presence (△) of 30 mol% cholesterol. The concentration of $Dipy_{10}PC$ was 0.1 mol%. The bars indicate the confidence limits of the fittings.

3-state model provides both the conformation and dynamics information. The values of the calculated K_{mm}/K_{mm} and K_{ds} are associated with the state of aggregation (conformation) and reorientational rate (rotational mobility) of the intralipid pyrene moieties, respectively, on the basis of the 3-state model. On the other hand, K_{dm} is related with a combination of the lateral and rotational mobility of pyrenes on the basis of the 2-state model. The value of K_{md} or K_{ds} calculated from the 2- or 3-state model, respectively, refers to the dissociation rate of dimer.

From the isotropic solution study, the values of K_{ds}, K_{dm}, and K_{mm} decrease with increasing chain length, indicating that the relative rotational and lateral diffusion rates of the covalently attached pyrene molecules at the ends of the chains becomes slower when the chain is getting longer. A slight decline in K_{mm}/K_{mm} of $Dipy_nPC$ with increasing n also indicates that the pyrene molecules are closer together for shorter chain length than for longer chain length. This probably reflects that the available conformational space or free volume for the pyrene molecules to form an excimer increases with increasing chain length of a dipyrenyl lipid (Cheng et al., 1991; Kodati and Lafleur, 1992; Pearce and Harvey, 1993).

In the bilayer membranes, the K_{ds} of either $Dipy_4PC$ or $Dipy_{10}PC$ increases dramatically by more than threefold at the L_β-L_α transition of DMPC, indicating that the rotational mobility of either short or long acyl chains is enhanced as the lipid membranes entering the disordered fluid phase from the

TABLE 3 Kinetic parameters (K_{da}, K_{ad}, K_{am}, and K_{ma}) of Dipy$_4$PC in DMPC, with and without 30 mol% cholesterol, at 15, 25, and 32°C

Sample	K_{da} ($10^7 s^{-1}$)	K_{ad} ($10^7 s^{-1}$)	K_{am} ($10^7 s^{-1}$)	K_{ma} ($10^7 s^{-1}$)	χ_3^2 (χ_2^2)	K_{am}/K_{ma}
DMPC (15°C)	5.06 (4.67, 5.49)	2.18	0.95 0.60, 1.50	0.06 (0.01, 0.14)	0.54 (0.55)	2.16 (4.28, 150)
DMPC/CHOL (15°C)	30.8 (25.7, 36.1)	6.85	0.80 (0.49, 1.16)	0.81 (0.48, 1.19)	1.80 (1.80)	0.99 (0.41, 2.41)
DMPC (25°C)	14.3 (18.2, 31.3)	0.61	4.71 (3.35, 12.8)	1.67 (1.83, 2.41)	1.32 (1.57)	2.82 (1.39, 7.01)
DMPC/CHOL (25°C)	14.8 (10.9, 19.4)	1.19	1.85 (1.51, 2.18)	1.08 (0.78, 1.37)	1.33 (1.87)	1.71 (1.10, 2.79)
DMPC (32°C)	22.4 (13.1, 36.0)	0.45	7.08 (5.83, 8.47)	3.42 (0.77, 7.34)	2.19 (2.39)	2.07 (0.79, 11.0)
DMPC/CHOL (32°C)	29.7 (18.8, 45.9)	0.95	2.98 (2.37, 3.57)	1.72 (1.17, 2.35)	3.19 (4.24)	1.73 (1.01, 3.05)

Values in parentheses are confidence limits. Confined 3-state fits (fixed K_{ad}) were used here. The fixed K_{ad} values were identical to those of K_{ma} obtained from the 2-state fits. The values of chi square of the 3- and 2-state fits are given by χ_3^2 and χ_2^2, respectively.

TABLE 4 Kinetic parameters (K_{da}, K_{ad}, K_{am}, and K_{ma}) of Dipy$_{10}$PC in DMPC, with and without 30 mol% cholesterol, at 15, 25, and 32°C

Sample	K_{da} ($10^7 s^{-1}$)	K_{ad} ($10^7 s^{-1}$)	K_{am} ($10^7 s^{-1}$)	K_{ma} ($10^7 s^{-1}$)	χ_3^2 (χ_2^2)	K_{am}/K_{ma}
DMPC (15°C)	3.77 (2.94, 4.66)	4.96	0.85 (0.43, 1.64)	0.17 (0.02, 0.34)	(0.82, 0.85)	5.00 (1.26, 82.0)
DMPC/CHOL (15°C)	22.8 (19.9, 23.6)	3.08	197 (59, 692)	3.12 (−2.3, 18.9)	0.31 (0.31)	63.1 (3.12, ∞)
DMPC (25°C)	19.9 (16.1, 24.5)	1.01	1.68 (1.58, 1.78)	1.98 (1.77, 2.19)	0.27* (0.81)	0.85 (0.72, 1.01)
DMPC/CHOL (25°C)	35.5 (31.3, 40.0)	2.11	2.65 (2.36, 2.94)	0.30 (0.21, 0.40)	0.35* (0.64)	8.83 (5.90, 14.0)
DMPC (32°C)	24.9 (20.1, 30.7)	0.71	2.86 (2.69, 3.03)	2.26 (1.97, 2.54)	0.28* (0.93)	1.27 (1.06, 1.54)
DMPC/CHOL (32°C)	43.2 (35.3, 51.6)	1.49	3.69 (3.41, 3.98)	0.78 (0.61, 0.96)	0.37* (0.94)	4.37 (3.55, 6.52)

Values in parentheses are confidence limits. Confined 3-state fits (fixed K_{ad}) were used here. The fixed K_{ad} values were identical to those of K_{ma} obtained from the 2-state fits. The values of chisquares of the 3-state and 2-state fits are given by χ_3^2 and χ_2^2, respectively. * Significant improvement in the 3-state fits over the 2-state fit ($p < 0.05$).

ordered gel phase. Interestingly, the K_{am}/K_{ma} of Dipy$_4$PC remains insensitive to the phase transition, whereas a significant decrease in the K_{am}/K_{ma} of Dipy$_{10}$PC is found at the transition. These results indicate that the conformational dynamics of the chains near the membrane surface remains relatively insensitive to the transition as compared with that near the center of the bilayer, and that the terminal methyl ends of the lipid acyl chains are much further apart in the liquid crystalline phase than those in the gel phase (De Loof et al., 1991).

In this study, lacks of improvement of the chi square of the 3-state fits over the 2-state fits, as well as the nonuniqueness of the free 3-state fits, for Dipy$_4$PC at all temperatures and Dipy$_{10}$PC in the gel phase of lipid membranes were reported. These results imply that the intralipid pyrene molecules in the above conditions are already quite close to each other (Sugar et al., 1991b). In this respect, a 1-step process ($\bar{A}^* \leftrightharpoons \bar{D}^*$), similar to the 2-state model, is already quite sufficient to describe the kinetics of the pyrene molecules as compared with the 2-step processes ($\bar{M}^* \leftrightharpoons \bar{A}^* \leftrightharpoons \bar{D}^*$) as depicted by the 3-state model (see Fig. 2).

The differential effects of cholesterol on the conformational dynamics of the short chain Dipy$_4$PC and long chain Dipy$_{10}$PC in DMPC lipid membranes are quite interesting. Cholesterol has a profound effect on various membrane physical properties such as permeability of small polar solutes, and it can also greatly modulate the activity and thermal stability of membrane bound enzymes (Demel et al., 1972; Yeagle, 1988; Cheng et al., 1986, 1987). Recent spectroscopy studies (Almeida et al., 1992, 1993) of DMPC/cholesterol membranes suggested that the lipids are in the liquid ordered phase at 30% cholesterol as used in this study. For the short chain Dipy$_4$PC in the gel phase of DMPC, K_{da} increases but the K_{am}/K_{ma} decreases in response to the presence of cholesterol. This suggests that the cholesterol causes the pyrene molecules of the short chain Dipy$_4$PC lipids to

become more separated apart and to rotate more faster. It is believed that the planar cholesterol molecule can even partition in between the pyrene molecules of the short chain $Dipy_4PC$ lipid to create the above effects. Surprisingly, this perturbing effect of cholesterol is not found when the lipid membranes enter the liquid crystalline phase. For the long chain $Dipy_{10}PC$, the drastic enhancement of K_{am}/K_{ma} and K_{da} in the presence of cholesterol suggests that cholesterol reduces the separation and allows faster rotation of the pyrene molecules of the long chain $Dipy_{10}PC$ lipids, probably by altering the intra- and intermolecular interactions (De Loof et al., 1991; Rey et al., 1992; Alam, 1993) among the chains near the center of the bilayer membranes. A feasible explanation for the enhanced K_{am}/K_{ma} is that cholesterol reduces the number of gauche bonds (Trouard et al., 1992; Song and Waugh, 1993) and thereby effectively straightens the longer acyl chains of $Dipy_{10}PC$. In this respect, the available conformational space (Cheng et al., 1991) of the covalently attached pyrene molecules is more limited, and results in an increase in the extent of intramolecular aggregation of pyrenes.

Our current site-specific intramolecular dynamics results complement the existence knowledge of the role of cholesterol on the intermolecular interactions, particularly lateral mobility (Almeida et al., 1992, 1993), organization (Hui, 1988; Finean, 1989), and thermodynamics properties (Needham et al., 1988; McMullen et al., 1994) of lipids in bilayer membranes. In addition, the calculated kinetic parameters of intramolecular pyrenes can provide some insight into the effects of lipid phase behavior and cholesterol on the molecular dynamics of membrane components, e.g., transmembrane domain of integral membrane proteins, in the nanosecond time regime. The numerical values of the kinetic parameters can also be useful for future molecular dynamics simulations or calculations of dipyrenyl lipids in membranes.

In conclusion, we have examined the conformation and rotational mobility of dipyrenyl lipids in isotropic solution and in anisotropic lipid bilayer membranes with and without the presence of cholesterol. The differential responses of the calculated intramolecular kinetic parameters of $Dipy_4PC$ and $Dipy_{10}PC$ on the phase transition and the presence of cholesterol further suggests the important potential of using nanosecond-resolved fluorescence measurements of $Dipy_nPC$ to probe the conformational dynamics of lipid bilayer membranes and native biological membranes. An investigation of the intramolecular dynamics of the acyl chains in lipid membranes exhibiting well defined composition-driven bilayer-to-nonbilayer transition and a discussion of the limitations of our proposed 3-state model are presented in a companion paper.

We would like to thank Dr. Michael L. Johnson, Department of Pharmacology and Internal Medicine at University of Virginia Health Sciences Center, for consultations and providing the source code of his nonlinear fitting subroutine from which our frequency-domain data fitting program was developed.

This work was supported by the Robert A. Welch Research Foundation (D-1158) and National Institutes of Health grant CA47610 given to K. H. Cheng and the Finnish Academy given to P. Somerharju.

APPENDIX

For the 2-state model, $\tilde{X}_1(\omega)$, $\tilde{X}_2(\omega)$, $m_E(\omega, \lambda_M)$, and $m_E(\omega, \lambda_D)$ are given by

$$\tilde{X}_1(\omega) = \frac{\begin{bmatrix} -1 & K_{md} \\ 0 & -K_d - K_{md} - i\omega \end{bmatrix}}{\begin{bmatrix} -K_m - K_{dm} - i\omega & K_{md} \\ K_{dm} & -K_d - K_{md} - i\omega \end{bmatrix}} \tag{A1}$$

$$\tilde{X}_2(\omega) = \frac{\begin{bmatrix} -K_m - K_{dm} - i\omega & -1 \\ K_{dm} & 0 \end{bmatrix}}{\begin{bmatrix} -K_m - K_{dm} - i\omega & K_{md} \\ K_{dm} & -K_d - K_{md} - i\omega \end{bmatrix}} \tag{A2}$$

$$m_E(\omega, \lambda_M) = \frac{\tilde{X}_1(\omega)}{\tilde{X}_1(0)} \qquad m_E(\omega, \lambda_D) = \frac{\tilde{X}_2(\omega)}{\tilde{X}_2(0)}. \tag{A3}$$

For the 3-state model, $\tilde{X}_1(\omega)$, $\tilde{X}_2(\omega)$, $\tilde{X}_3(\omega)$, $m_E(\omega, \lambda_M)$, and $m_E(\omega, \lambda_D)$ are given by

$$\tilde{X}_1(\omega) = \frac{\begin{bmatrix} -1 & K_{am} & 0 \\ -K_{am}/K_{ma} & -K_m - K_{am} - K_{da} - i\omega & K_{ad} \\ 0 & K_{da} & -K_d - K_{ad} - i\omega \end{bmatrix}}{\begin{bmatrix} -K_m - K_{am} - i\omega & K_{am} & 0 \\ K_{am} & -K_m - K_{am} - K_{da} - i\omega & K_{ad} \\ 0 & K_{da} & -K_d - K_{ad} - i\omega \end{bmatrix}} \tag{A4}$$

$$\tilde{X}_2(\omega) = \frac{\begin{bmatrix} -K_m - K_{am} - i\omega & -1 & 0 \\ -K_{am} & -K_{am}/K_{ma} & K_{ad} \\ 0 & 0 & -K_d - K_{ad} - i\omega \end{bmatrix}}{\begin{bmatrix} -K_m - K_{am} - i\omega & K_{am} & 0 \\ K_{am} & -K_m - K_{am} - K_{da} - i\omega & K_{ad} \\ 0 & K_{da} & -K_d - K_{ad} - i\omega \end{bmatrix}} \tag{A5}$$

$$\tilde{X}_3(\omega) = \frac{\begin{bmatrix} -K_m - K_{am} - i\omega & K_{am} & -1 \\ -K_{am} & -K_m - K_{am} - K_{da} - i\omega & -K_{am}/K_{ma} \\ 0 & K_{da} & 0 \end{bmatrix}}{\begin{bmatrix} -K_m - K_{am} - i\omega & K_{am} & 0 \\ K_{am} & -K_m - K_{am} - K_{da} - i\omega & K_{ad} \\ 0 & K_{da} & -K_d - K_{ad} - i\omega \end{bmatrix}}. \tag{A6}$$

$$m_E(\omega, \lambda_M) = \frac{\tilde{X}_1(\omega) + \tilde{X}_2(\omega)}{\tilde{X}_1(0) + \tilde{X}_2(0)} \qquad m_E(\omega, \lambda_D) = \frac{\tilde{X}_3(\omega)}{\tilde{X}_3(0)} \tag{A7}$$

REFERENCES

Alam, T. M. 1993. Molecular dynamics in lipid bilayers. Anisotropic diffusion in an odd restoring potential. *Biophys. J.* 64:1681–1690.

Almeida, P. F. F., W. L. C. Vaz, and T. E. Thompson. 1992. Lateral diffusion in liquid phases of dimyristoylphosphatidylcholine/cholesterol lipid bilayers: a free volume analysis. *Biochemistry.* 31:6739–6747.

Almeida, P. F. F., W. L. C. Vaz, and T. E. Thompson. 1993. Percolation and diffusion in three-component lipid bilayers: effect of cholesterol on an equimolar mixture of two phosphatidylcholines. *Biophys. J.* 64:399–412.

Ameloot, M., J. M. Beechem, and L. Brand. 1986. Compartmental modeling of excited-state reactions: identifiability of the rate constants from fluorescence decay surfaces. *Chem. Phys. Lett.* 129:211–219.

Bloom, M. F., and E. Sternin. 1987. Transverse nuclear spin relaxation in phospholipid bilayer membranes. *Biochemistry.* 26:2101–2105.

Brown, M. F., A. A. Ribeiro, and G. D. Williams. 1983. New view of lipid bilayer dynamics from ^2H and ^{13}C NMR relaxation time measurements. *Proc. Natl. Acad. Sci. USA.* 80:4325–4329.

Birks, J. B., D. J. Dyson, and I. H. Munro. 1963. "Excimer" fluorescence II. Lifetime studies of pyrene solutions. *Proc. R. Soc. Lond.* 275:575–588.

Chen, S.-Y., K. H. Cheng, B. W. Van Der Meer, and J. M. Beechem. 1990a. Effects of lateral diffusion on the fluorescence anisotropy in hexagonal lipid phase II. An experimental study. *Biophys. J.* 58:1527–1537.

Chen, S.-Y., K. H. Cheng, and D. M. Ortalano. 1990b. Lateral diffusion study of excimer forming lipids in lamellar to inverted hexagonal phase

transition of unsaturated phosphatidylethanolamine. *Chem. Phys. Lipids.* 53:321–330.

Chen, S.-Y., K. H. Cheng, and B. W. Van Der Meer. 1992. Quantitation of lateral stress in lipid layer containing nonbilayer phase preferring lipids by frequency-domain fluorescence spectroscopy. *Biochemistry.* 31: 3759–3768.

Cheng, K. H. 1989a. Fluorescence depolarization study of lamellar liquid crystalline to inverted cylindrical micellar phase transition of phosphatidylethanolamine. *Biophys. J.* 55:1025–1031.

Cheng, K. H. 1989b. Fluorescence depolarization study on non-bilayer phases of phosphatidylethanolamine and phosphatidylcholine lipid mixtures. *Chem. Phys. Lipids.* 51:137–145.

Cheng, K. H. 1989c. Time-resolved fluorescence depolarization study of lamellar to inverted cylindrical micellar phase. *Proc. SPIE Int. Soc. Opt. Eng.* 1054:160–167.

Cheng, K. H., S.-Y. Chen, P. Butko, B. W. Van Der Meer, and P. Somerharju. 1991. Intramolecular excimer formation of pyrene-labeled lipids in lamellar and inverted hexagonal phases of lipid mixtures containing unsaturated phosphatidylethanolamine. *Biophys. Chem.* 39:137–144.

Cheng, K. H., S. W. Hui, and J. R. Lepock. 1987. Protection of membrane calcium adenosine triphosphatase by cholesterol from thermal inactivation. *Cancer Res.* 47:1255–1262.

Cheng, K. H., and J. R. Lepock. 1992. Inactivation of calcium uptake by EGTA is due to an irreversible thermotropic conformational change in the calcium binding domain of the Ca^{2+}-ATPase. *Biochemistry.* 31: 4074–4080.

Cheng, K. H., J. R. Lepock, S. W. Hui, and P. L. Yeagle. 1986. The role of cholesterol in the activity of reconstituted Ca-ATPase vesicles containing unsaturated phosphatidylethanolamine. *J. Biol. Chem.* 261: 5081–5087.

Chong, P. L., and T. E. Thompson. 1985. Oxygen quenching of pyrene-lipid fluorescence in phosphatidylcholine vesicles. A probe for membrane organization. *Biophys. J.* 47:613–621.

Davenport, L., J. R. Knutson, and L. Brand. 1986. Excited-state proton transfer of equilenin and dihydroequilenin: interaction with bilayer vesicles. *Biochemistry.* 25:1186–1195.

De Loof, H., S. C. Harvey, J. P. Segrest, and R. W. Pastor. 1991. Mean field stochastic boundary molecular dynamics simulation of a phospholipid in a membrane. *Biochemistry.* 30:2099–2113.

Demel, R. A., K. R. Bruckdorfer, and L. L. M. Van Deenen. 1972. The effect of sterol structure on the permeability of liposomes to glucose, glycerol and Rb. *Biochim. Biophys. Acta.* 255:321–330.

Eklund, K. K., J. A. Virtanen, P. K. J. Kinnunen, J. Kasurinen, and P. J. Somerharju. 1992. Conformation of phosphatidylcholine in neat and cholesterol containing crystalline bilayers. Application of a novel method. *Biochemistry.* 31:8560–8565.

Finean, J. B. 1989. X-ray diffraction studies of lipid phase transitions in hydrated mixtures of cholesterol and diacylphosphatidylcholines and their relevance to the structure of biological membranes. *Chem. Phys. Lipids.* 49:265–269.

Gratton, E., D. M. Jameson, and R. D. Hall. 1984. Multifrequency phase and modulation fluorometry. *Annu. Rev. Biophys. Bioeng.* 13:105–124.

Hresko, R. C., I. P. Sugar, Y. Barenholz, and T. E. Thompson. 1986. Lateral Distribution of a Pyrene-labeled phosphatidylcholine in phosphatidylcholine bilayers: fluorescence phase and modulation study. *Biochemistry.* 25:3813–3823.

Hui, S. W. 1988. The spatial distribution of cholesterol in membranes. *In* Biology of Cholesterol. P. L. Yeagle, editor. CRC Press, Boca Raton, FL. 213 pp.

Johnson, M. L. 1983. Evaluation and propagation of confidence intervals in nonlinear, asymmetrical variance spaces: analysis of ligand binding data. *Biophys. J.* 44:101–106.

Knao, K., H. Kawazumi, T. Ogawa, and J. Sunamoto. 1981. Fluorescence quenching in liposomal membranes. Exciplex as a probe for investigating artificial lipid membrane properties. *J. Phys. Chem.* 85:2204–2209.

Kodati, V. R., and M. Lafleur. 1992. Comparison between orientational and conformational orders in fluid lipid bilayers. *Biophys. J.* 64:163–170.

Lakowicz, J. R. 1983. Principle of Fluorescence Spectroscopy. Plenum Press, New York. 126 pp.

Lepock, J. R., Rodahl, A. M., C. Zhang, M. L. Heynen, B. Waters, and K. H. Cheng. 1990. Thermal denaturation of the Ca^{2+}-ATPase of sarcoplasmic reticulum reveals two thermodynamically independent domains. *Biochemistry.* 29:681–689.

Liu, L., K. H. Cheng, and P. Somerharju. 1993. Frequency-resolved intramolecular excimer fluorescence study of lipid bilayer and non-bilayer phases. *Biophys. J.* 64:1869–1877.

MacLennan, D. H. 1990. Molecular tools to elucidate problems in excitation-contraction coupling. *Biophys. J.* 58:1355–1365.

McMullen, T. P. W., R. N. A. H. Lewis, and R. N. McElhaney. 1994. Comparative differential scanning calorimetric and FTIR and ^{31}P-NMR spectroscopic studies of the effect of cholesterol and androsterol on the thermotropic phase behavior and organization of phosphatidylcholine bilayers. *Biophys. J.* 66:741–752.

Melnick, R. L., H. C. Haspel, M. Goldenberg, Greenbaum, L. M., and S. Weinstein. 1981. Use of fluorescent probes that form intramolecular excimer to monitor changes in model and biological membranes. *Biophys. J.* 34:499–515.

Needham, D., T. J. McIntosh, and E. Evans. 1988. Thermodynamical and transition properties of DMPC/cholesterol bilayers. *Biochemistry.* 27:4668–4673.

Patel, K. M., J. D. Morrisett, and J. T. Sparrow. 1979. A convenient synthesis of phosphatidylcholine acylation of *sn*-glycero-3-phosphocholine with fatty acid anhydride and 4-pyrrolidinopyrine. *J. Lipid Res.* 20:674–677.

Pearce, L. L., and S. C. Harvey. 1993. Langevin dynamics studies of unsaturated phospholipids in a membrane environment. *Biophys. J.* 65:1084–1092.

Peng, Z.-Y., V. Simplaceanu, I. J. Lowe, and C. Ho. 1988. Rotating-frame relaxation studies of slow motions in fluorinated phospholipid model membranes. *Biophys. J.* 54:81–95.

Rey, A., A. Kolinski, J. Skolnick, and Y. K. Levine. 1992. Effect of double bonds on the dynamics of hydrocarbon chains. *J. Chem. Phys.* 92: 1240–1249.

Sassaroli, M., M. Vauhkonen, P. Somerharju, and S. Scarlata. 1993. Dipyrenylphosphatidylcholines as membrane fluidity probe. Pressure and temperature dependence of the intramolecular rate. *Biophys. J.* 64:137–149.

Song, J., and R. E. Waugh. 1993. Bending rigidity of SOPC membranes containing cholesterol. *Biophys. J.* 64:1967–1970.

Sugar, I. P. 1991. Use of fourier transforms in the analysis of fluorescence data. 1. A general method for finding explicit relationships between photophysical models and fluorescence parameters. *J. Phys. Chem.* 95: 7508–7515.

Sugar, I. P., J. Zeng, M. Vauhkonen, P. Somerharju, and P. L.-G. Chong. 1991a. Use of fourier transforms in the analysis of fluorescence data. 2. Fluorescence of pyrene-labeled phosphatidylcholine in lipid bilayer membrane. Test of the Birks model. *J. Phys. Chem.* 95:7516–7523.

Sugar, I. P., J. Zeng, and P. L.-G. Chong. 1991b. Use of fourier transforms in the analysis of fluorescence data. 3. Fluorescence of pyrene-labeled phosphatidylcholine in lipid bilayer membrane. A three-state model. *J. Phys. Chem.* 95:7524–7534.

Trouard, T. P., T. M. Alam, J. Zajicek, and M. F. Brown. 1992. Angular anisotropy of 2H NMR spectral densities in phospholipid bilayers containing cholesterol. *Chem. Phys. Lett.* 189:67–75.

Vauhkonen, M., M. Sassaroli, P. Somerharju, and J. Eisinger. 1990. Dipyrenylphosphatidylcholines as membrane fluidity probes. Relationship between intramolecular and intermolecular excimer formation rates. *Biophys. J.* 57:291–300.

Yeagle, P. L. 1988. The biology of cholesterol. *In* Biology of Cholesterol. P. L. Yeagle, editor. CRC Press, Boca Raton, FL. 242 pp.